Materials Letters 256 (2019) 126628

Contents lists available at ScienceDirect

Materials Letters

journal homepage: www.elsevier.com/locate/mlblue

Investigation on metallic glass formation in Mg-Zn-Sr ternary system combined with the CALPHAD method

Jian Wang [a,b,c], Zhang Zhang [a,b], Yi-Nan Zhang [d], Dong Han [a,b], Liling Jin [c], Liyuan Sheng [b,*], Patrice Chartrand [c], Mamoun Medraj [e]

[a] School of Mechanical Engineering, Yangzhou University, Yangzhou 225009, China
[b] Shenzhen Institute, Peking University, Shenzhen 518057, China
[c] Center for Research in Computational Thermochemistry (CRCT), Dept. of Chemical Engineering, École Polytechnique, H3C 3A7, Canada
[d] Institute of Biomaterials and Biomedical Engineering, University of Toronto, Toronto M5S 3G9, Canada
[e] Department of Mechanical Engineering, Concordia University, 1455 De Maisonneuve Blvd. West, Montreal H3G 1M8, Canada

ARTICLE INFO

Article history:
Received 4 August 2019
Received in revised form 2 September 2019
Accepted 4 September 2019
Available online 4 September 2019

Keywords:
CALPHAD
Mg-Zn-Sr alloys
Metallic glass

ABSTRACT

Glass forming ability (GFA) of Mg-Zn alloys with Sr addition has been experimentally studied coupled with CALPHAD method. Two series of metallic glasses (MGs), $Mg_{98-x}Zn_xSr_2$ (x = 38, 36, 33, 30, 28) and $Mg_{95-x}Zn_xSr_5$ (x = 37, 33, 30, 27, 23), were designed and prepared successfully for the first time. The crystallization characteristics of these MGs were investigated by differential scanning calorimetry (DSC), X-ray diffraction (XRD). All results indicate that the extraordinary GFA should locate at the composition regions of $Mg_{68}Zn_{27}Sr_5$ to $Mg_{60}Zn_{35}Sr_5$ for $Mg_{95-x}Zn_xSr_5$, and $Mg_{68}Zn_{30}Sr_2$ to $Mg_{64}Zn_{34}Sr_2$ for $Mg_{98-x}Zn_xSr_2$, respectively.

1. Introduction

Mg alloys with excellent biocompatibility have become one of the most revolutionary research topics as bio-implant materials [1]. However, the clinic applications are limited with the current developed Mg alloys due to their high corrosion rate and hydrogen release rate [2]. Mg-Zn-Ca based bulk metallic glasses have received considerable attention because of their much lower corrosion rate and good mechanical properties [3]. Unfortunately, the brittleness of Mg-Zn-Ca MGs and poor GFA have hindered their further application [4]. Thus, it is desirable to develop new Mg-based MGs with superior GFA and mechanical properties. Strontium, a bone-seeking element, has been reported to be capable of stimulating bone-cells replication and protein synthesis, depressing bone resorption, and increasing bone mass and strength [5,6]. Hence, it is necessary to develop MGs of the Mg-Zn-Sr system with superior biocompatibility.

The production of MGs is relied on the inhibition of crystalline phase(s) formation using fast solidification process. The composition with relatively lower nuclear driving forces (NDFs), resulting less ability of crystalline phase(s) formation, indicates a super GFA of alloys. Thermodynamic modeling of phase equilibria via CALPHAD technique enables calculating the NDFs of crystalline phases, which can be used to search the composition of Mg-Zn-Sr alloys with superior GFA. Therefore, in this work, the GFA of Mg-Zn-Sr alloys were studied experimentally combined CALPHAD technique for biomaterials application purpose.

2. Experimental procedure

Ten samples in total of $Mg_{98-x}Zn_xSr_2$ (x = 38, 36, 33, 30, 28) and $Mg_{95-x}Zn_xSr_5$ (x = 37, 33, 30, 27, 23) were prepared. All samples were prepared by melting high-purity Mg ingot of 99.8%, Sr of 99%, and Zn of 99.99% in an induction furnace. All the samples were melted at least 3 times in a cubic shaped Ta foil crucible under an argon atmosphere to reach good homogeneity. The mass losses of the elements during melting have been taken into account during the weighting, and they were controlled within 1 wt% for each sample. Then, samples were cut into pieces for single-roller melt-spinning. The melt-spinning process was carried out under high purity helium protective atmosphere (at a pressure of 50 kPa) with a wheel tangential speed of 50 m/s. The XRD technique was used to verify the amorphous state on the free side of each ribbon. XRD patterns were obtained using PANanalytical X'pert Pro powder X-ray diffractometer with a CuKα radiation at 45 kV and 40 mA. The XRD spectrum was acquired from 20 to 120° 2θ with a 0.02° step size. The thermal properties of the as-quenched glassy

* Corresponding author.
E-mail address: lysheng@yeah.net (L. Sheng).

https://doi.org/10.1016/j.matlet.2019.126628
0167-577X/

samples were studied by calibrated non-isothermal DSC from SETARAM instrumentation under a continuous flow of purified argon. All the samples were tested in a graphite crucible covered with lid at the heating rates of 5, 10, 20 and 40 K/min.

3. Results and discussion

The NDFs of crystalline phases of Mg-Zn system are calculated as a function of Zn content at 340 °C (Fig. 1a), at which the alloys correspond to super-cooled liquids. Along with the varying of Zn content, the NDFs of crystalline phases show a "V" shape with the minimum value at the composition around $Mg_{71}Zn_{29}$ having the superior GFA. Present calculated result is in a good agreement with the reported value of $Mg_{70}Zn_{30}$ [7,8].

The NDFs of crystalline phases in Mg-Zn-Sr ternary system at 340 °C were calculated with constant values of 2 and 5 at. % Sr as shown in Fig. 1b and c. The "V" shape of NDFs with minimum point locates at compositions of $Mg_{68}Zn_{30}Sr_2$ and $Mg_{63}Zn_{32}Sr_5$, respectively, where indicates the superior GFA of MGs.

Based on the present prediction, ten samples with compositions of $Mg_{98-x}Zn_xSr_2$ (x = 38, 36, 33, 30, 28) and $Mg_{95-x}Zn_xSr_5$ (x = 37, 33, 30, 27, 23) were selected for MGs preparation. The XRD patterns of free side part of the as-quenched Mg-Zn-Sr MGs obtained by the melt-spinning method are shown in Fig. 2. The absence of detectable crystalline diffraction peaks, together with the broad scattering peaks at 2θ = 38° to 66°, confirms the amorphous nature of these samples except the sample A1 ($Mg_{70}Zn_{28}Sr_2$). By increasing the Zn content, the broad scattering maxima shift slightly towards higher diffraction angles because Zn atom have a smaller atomic radius than Mg. The appearance of little peaks in the XRD pattern indicates that A1 is not homogenous glass.

The "strong liquid" behavior of metallic glasses results in a reduced rate of both crystal nucleation and growth, therefore contributes greatly to the extraordinary GFA [9]. Here, the glass transition temperature (T_g), melting temperature (T_m), and crystallization temperatures (T_{p1}, T_{p2}, T_{p3}...) are used to evaluate the GFA of MGs. The composition dependence of characteristic temperatures: T_g, T_m, T_{p1}, T_{p2}, and T_{p3} measured using DSC with constant heating rate of 5 K/min in the present work are shown in Fig. 3a, and results obtained from the other heating rates (10, 20, and 40 K/min) are listed in the Table 1. The minimum values of melting temperature changes were determined to be $Mg_{65}Zn_{33}Sr_2$ and $Mg_{65}Zn_{28}Sr_5$. The composition dependence of the reduced glass transition temperature T_{rg} ($T_{rg} = T_g/T_M$) of the two series samples with constant heating rate of 5 K/min are shown in Fig. 3b. These measured results indicated that the extraordinary GFA should locate at the composition regions of $Mg_{68}Zn_{27}Sr_5$ to $Mg_{60}Zn_{35}Sr_5$ for $Mg_{95-x}Zn_xSr_5$, and $Mg_{68}Zn_{30}Sr_2$ to $Mg_{64}Zn_{34}Sr_2$ for $Mg_{98-x}Zn_xSr_2$. Moreover, the $Mg_{95-x}Zn_xSr_5$ alloys have larger formation range and more superior GFA of MGs comparing with $Mg_{98-x}Zn_xSr_2$ alloys.

The heating rate dependence of crystallization of phase in metallic glass indicates that the nucleation and phase formation are thermally activated process, whereas the rate dependence of

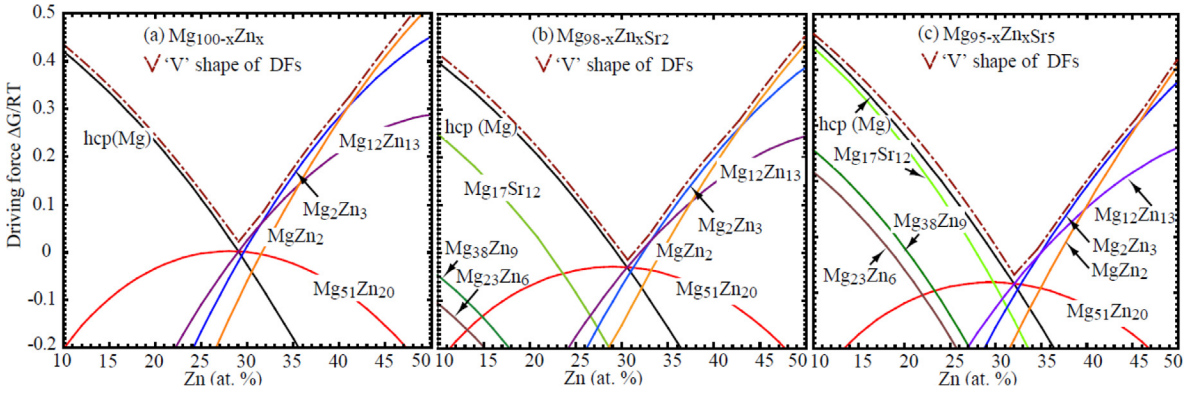

Fig. 1. The calculated DFs of individual crystalline phases of (a) Mg-Zn, (b) $Mg_{98-x}Zn_xSr_2$ and (c) $Mg_{95-x}Zn_xSr_5$ alloys using CALPHAD technique.

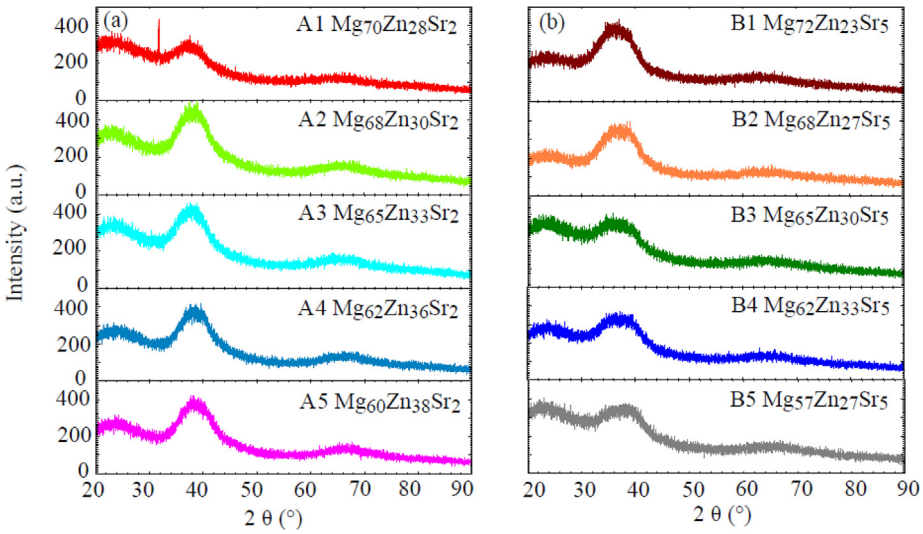

Fig. 2. The XRD patterns of free side parts of the as-quenched Mg–Zn–Sr MGs: (a) $Mg_{98-x}Zn_xSr_2$ and (b) $Mg_{95-x}Zn_xSr_5$ alloys obtained by the melt-spinning method.

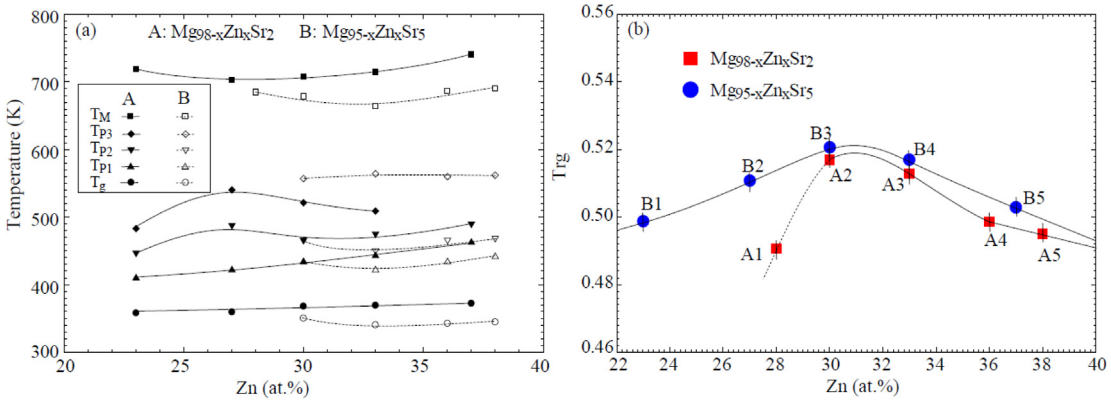

Fig. 3. The composition dependence of (a) characteristic temperatures: T_g, T_m, T_{p1}, T_{p2}, and T_{p3}; (b) reduced glass transition temperature T_{rg} measured of $Mg_{98-x}Zn_xSr_2$ and $Mg_{95-x}Zn_xSr_5$ MGs using DSC measurements with constant heating rate of 5 K/min.

Table 1
Characteristic temperatures and activation energies for crystallization of $Mg_{98-x}Zn_xSr_2$ (x = 38, 36, 33, 30) and $Mg_{95-x}Zn_xSr_5$ (x = 37, 33, 30, 27, 23) metallic glass.

Sample	Crystallization temperature (K)	Heating rate (K/min)				Activation energy (kJ/mol)	
		5	10	20	40		
$Mg_{68}Zn_{30}Sr_2$ (A2)	T_{p1}	433	437	440	443	E_{p1}	331.8
	T_{p2}	464	469	473	477	E_{p2}	296.3
$Mg_{65}Zn_{33}Sr_2$ (A3)	T_{p1}	422	425	427	433	E_{p1}	350.4
	T_{p2}	449	455	461	466	E_{p2}	271.7
$Mg_{62}Zn_{36}Sr_2$ (A4)	T_{p1}	434	437	440	443	E_{p1}	341.9
	T_{p2}	463	468	473	477	E_{p2}	262.1
$Mg_{60}Zn_{38}Sr_2$ (A5)	T_{p1}	442	445	448	452	E_{p1}	339.8
	T_{p2}	463	468	473	478	E_{p2}	247.3
$Mg_{72}Zn_{23}Sr_5$ (B1)	T_{p1}	410	413	419	423	E_{p1}	212.0
	T_{p2}	446	454	460	464	E_{p2}	186.4
$Mg_{68}Zn_{27}Sr_5$ (B2)	T_{p1}	422	426	430	436	E_{p1}	221.2
	T_{p2}	487	495	501	509	E_{p2}	189.5
$Mg_{65}Zn_{30}Sr_5$ (B3)	T_{p1}	434	437	442	446	E_{p1}	262.6
	T_{p2}	465	468	474	480	E_{p2}	239.5
$Mg_{62}Zn_{33}Sr_5$ (B4)	T_{p1}	443	448	453	457	E_{p1}	239.9
	T_{p2}	474	478	485	489	E_{p2}	245.5
$Mg_{58}Zn_{37}Sr_5$ (B5)	T_{p1}	464	467	475	478	E_{p1}	237.9
	T_{p2}	489	496	502	507	E_{p2}	228.3

*Note: Tp1 and Tp2 are crystallization peak temperatures, Ep1 and Ep2 are activation energies.

the kinetic glass transition temperature (T_g) is due to the relaxation process in the glass transition region. The apparent activation energy of each characteristic transformation was evaluated by Kissinger method [10]. The Kissinger Equation is based on the shift of the DSC curves with respect to different heating rates: $Ln\ (B/T^2) = -E/RT + C$, where E is the apparent activation energy (AE), B is the heating rate, R is the gas constant, C is a constant and T is the characteristic temperature such as T_{p1} and T_{p2} indicated on the DSC curves. The corresponding values of the characteristic temperatures and calculated AE are listed in Table 1. Whereas the 2nd crystallization E_{p2} includes the growth of nuclei. The compositions with higher E_{p1} should have higher resistance against crystallization, which results in superior GFA. The maximum E_{p1} obtained from the $Mg_{65}Zn_{33}Sr_2$ and $Mg_{65}Zn_{30}Sr_5$ alloys indicates the best thermal stability of MGs compared to other samples. These results show great consistency with the findings (Fig. 3b) obtained from the reduced glass transition temperature T_{rg}.

4. Conclusions

In summary, firstly, the method to prediction GFA via calculating and minimizing NDFs of crystalline compounds using CALPHAD technique was justified. In general, the composition with superior GFA is closely related with minimum point of "V" shape of crystalline phases NDFs. Moreover, two series of MGs: $Mg_{98-x}Zn_xSr_2$ (x = 38, 36, 33, 30, 28) and $Mg_{95-x}Zn_xSr_5$ (x = 37, 33, 30, 27, 23) were designed and prepared successfully for the first time. The crystallization characteristics of these two series of MGs were studied using DSC and XRD techniques. All results indicate that the extraordinary GFA should locates at the composition regions of $Mg_{68}Zn_{27}Sr_5$ to $Mg_{60}Zn_{35}Sr_5$ for $Mg_{95-x}Zn_xSr_5$, and $Mg_{68}Zn_{30}Sr_2$ to $Mg_{64}Zn_{34}Sr_2$ for $Mg_{98-x}Zn_xSr_2$.

Declaration of Competing Interest

The authors declare that they have no known competing financial interests or personal relationships that could have appeared to influence the work reported in this paper.

Acknowledgement

Financial supports from the Natural Science Foundation of Jiangsu Province (No. BK20160958), Natural Science Foundation of Guangdong Province, China (No. 2018A030313950), the Science and Technology Project of Shenzhen, China (Nos. JCYJ20170815153210359 and JCYJ20170306141749970) and General Motors of Canada Ltd. are gratefully acknowledged.

References

[1] X.-N. Gu, S.-S. Li, X.-M. Li, Y.-B. Fan, Magnesium based degradable biomaterials: a review, Front. Mater. Sci. 8 (2014) 200–218.
[2] M. Razavi, M. Fathi, O. Savabi, M. Boroni, A review of degradation properties of Mg based biodegradable implants, Res. Rev. Mater. Sci. Chem. 1 (2012) 15–58.
[3] S.Y. Cho, S.W. Chae, K.W. Choi, H.K. Seok, Y.C. Kim, J.Y. Jung, et al., Biocompatibility and strength retention of biodegradable Mg-Ca-Zn alloy bone implants, J. Bio. Mater. Res. B 101 (2013) 201–212.
[4] Q.F. Li, H.R. Weng, Z.Y. Suo, Y.L. Ren, X.G. Yuan, K.Q. Qiu, Microstructure and mechanical properties of bulk Mg-Zn-Ca amorphous alloys and amorphous matrix composites, Mater. Sci. Eng. A 487 (2008) 301–308.
[5] Y. Li, C. Wen, D. Mushahary, R. Sravanthi, N. Harishankar, G. Pande, et al., Mg–Zr–Sr alloys as biodegradable implant materials, Acta Biomater. 8 (2012) 3177–3188.
[6] Y. Ding, Y. Li, J. Lin, C. Wen, Effects of zirconium and strontium on the biocorrosion of Mg-Zr-Sr alloys for biodegradable implant applications, J. Mater. Chem. B. 3 (2015) 3714–3729.
[7] Z. Altounian, T. Guo-Hua, J. Strom-Olsen, The crystallization characteristics of Mg-Zn metallic glasses from $Mg_{80}Zn_{20}$ to $Mg_{60}Zn_{40}$, J. Mater. Sci. 17 (1982) 3268–3274.
[8] A. Calka, The room temperature stability of amorphous Mg-Zn alloys, J. Phys. F 16 (1986) 1577.
[9] J.F. Löffler, Bulk metallic glasses, Intermetallics 11 (2003) 529–540.
[10] H.E. Kissinger, Reaction kinetics in differential thermal analysis, Anal. Chem. 29 (1957) 1702–1706.